J. Fluid Mech. (1986), *vol.* 172, *pp.* 127–141
Printed in Great Britain

A gas jet impacting a cavity

By A. KENT STIFFLER
Mechanical Engineering Department, Mississippi State University, MS 39762, USA
AND HAZOOR BAKHSH
Research Institute, University of Petroleum and Minerals, Dhahran, Saudi Arabia

(Received 14 May 1984 and in revised form 16 December 1985)

A subsonic air jet impinging upon a cavity is studied to explain the resultant heating phenomenon. Flow visualization within the cavity shows a large central vortex dominating the flow pattern. Velocity measurements inside the cavity are made using a hot-wire anemometer. Temperature is measured with a copper–constantan thermocouple. The velocity field within the cavity is described by a modified Rankine combined vortex. An uncommon form of the energy equation is used to account for turbulent heating in adverse pressure gradients. A theoretical solution is developed to model the temperature field in the cavity. There is a good agreement between the calculated and measured temperatures. The heating effect is related to Ranque–Hilsch tubes.

1. Introduction

This paper addresses the subject of a subsonic gas jet impacting a cavity of comparable diameter, figure 1. There is no previous work reported in the literature describing the temperature and flow fields within such a cavity. The study was motivated by the heating phenomenon that occurs in 'resonance tubes' (cavities) where a jet is supersonic, and in the Ranque–Hilsch vortex tube.

While studying underexpanded air jets from simple convergent nozzles Hartmann (1931) discovered that a closed-end tube (Pitot tube) facing the jet will produce high-frequency oscillations when placed at selected locations from the nozzle. The flow accelerates to supersonic speed after emerging from the nozzle. It then returns to subsonic speed through a compression shock wave. The result is a series of stationary conical shock waves along the jet axis. When a tube or cavity is placed near one of these shock waves, self-sustaining oscillations are set up by resonant waves within the tube. These resonant shock waves travel up the jet to reflect at the nozzle exit. The resultant shifting of the conical shock waves within the jet produces the high intensity sound (Hartmann whistle). The use of schlieren photographs by Hartmann (1931), Brun & Boucher (1957), Thompson (1964) and others clearly shows that the main flow periodically charges and discharges the tube.

Sprenger (1954) was the first investigator to discover the thermal properties of the Hartmann oscillator, calling it a resonance tube. He excited the resonance tube (50 cm long and 1.25 cm diameter) with a 1.25 cm diameter air jet. Using a jet velocity of Mach 1.92 at the nozzle exit, he measured a temperature rise of 425 °C at the tube end. Rakowsky, Corrado & Marchese (1974) reported substantial increases in the endwall temperature with tapered and stepped resonance tubes. Przirembel & Fletcher (1977, 1978) found endwall temperatures increasing with the length/diameter ratio of the tube.

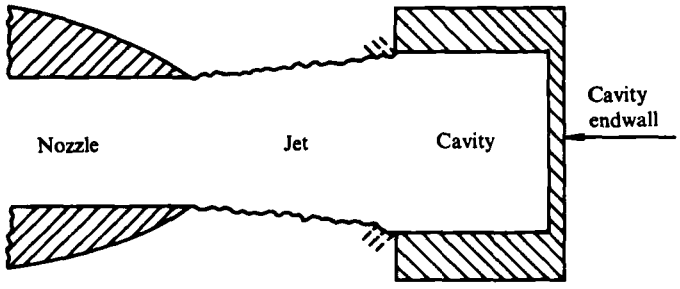

FIGURE 1. Air jet impacting a cavity.

The above heating phenomenon has been qualitatively explained by most authors in terms of periodic compression and expansion waves in the resonance tube. If a small portion of the gas is retained at the endwall and undergoes irreversible cycling, the resultant lost work would appear as heat. However, Sibulkin (1963) has calculated that the shock wave dissipation is approximately an order of magnitude less than is necessary to explain the measured temperature rise. Thompson (1964), Kang (1964), and Broucher, Maresca & Bournay (1970) have constructed rather elaborate wave diagrams within the tube to predict the high temperatures. Only order of magnitude estimations of the heat effect have been obtained.

Sprenger (1954) suggested a possible link between the resonance tube and the equally complex phenomenon, the Ranque–Hilsch effect. Others have not drawn this analogy. When compressed air is injected tangentially into a pipe, the total temperature of the vortex flow near the centre becomes cold while the total temperature of the air near the periphery exceeds the total temperature of the incoming air. The device was first patented by Ranque (1934) and later investigated by Hilsch (1947). It is known as the Ranque–Hilsch tube or vortex tube. They attributed the effect to axial expansion of the counterflowing central core.

There are numerous interpretations in the literature for the temperature difference produced in the vortex tube. All agree that the air in the core is cooled through adiabatic expansion and that the air in the outer region is heated through centrifugal pressure. There is a difference of opinions in the explanation of the transfer of energy from the vortex core to the wall and in the axial direction. Kassner & Knoernschild (1948) proposed a turbulent heat transfer theory in which heat is transferred against the temperature gradient in the radial direction. Turbulent 'packets' of fluid are fluxed first into the pressure gradient where they are adiabatically compressed and lose heat to the near fluid. When the 'packets' are fluxed toward the centre, the resultant expansion cools the fluid, and it takes on heat energy. The process is similar to a miniature heat pump. This concept was applied analytically to the Ranque–Hilsch tube by Deissler & Perlmutter (1960), and by Linderstrom-Lang (1971).

Recently Kurosaka (1982) has attributed the Ranque–Hilsch effect to the vortex whistle which accompanies the swirling flow. The tone induces a steady streaming of the radial flow which increases the swirl and leads to an increase in the total temperature. Also, Stephan *et al.* (1983) have proposed the Gortler vortex produced by the tangential velocity on the inside wall as the driving force for energy separation.

The current controversy over the heating effect in resonance tubes is due to the flow complexities and experimental problems associated with velocities that approach or exceed sonic conditions. Measurements have been confined to dynamic pressures

along the tube, endwall temperatures, and schlieren shock waves. Thus, it was decided to investigate subsonic jets to learn more of the flow behaviour within the cavities although it is recognized that the subsonic jet and cavity may operate under a different mechanism. The following experimental approaches were undertaken first. A theory evolved from the experimental findings.

2. Experiments

2.1. *General trends*

Since the Ranque–Hilsch tube requires a vortex to separate energy, it was likely that a vortex exists within the cavity impacted by the jet. The type of vortex motion could be strongly influenced by the cavity to nozzle diameter ratio (D/d). If the cavity diameter is much smaller than the jet diameter, it behaves as an impact tube. If the jet diameter is much smaller than the cavity diameter, it simply reverses at the cavity bottom. However, a jet which is small enough to enter a cavity, but has insufficient room to turn and leave, would seem to offer the best opportunity for a vortex motion. Most resonance tube studies have been done with equal jet and cavity diameters. Phillips & Pavli (1971) reported that endwall temperatures peaked in resonance tubes for a D/d ratio of 1.25.

A Thermo-System Model 1125 hot-wire anemometer calibrator conveniently provided a nozzle with a 0.38 cm diameter (and a 1.65 cm nozzle for later measurements). The device had a number of ports for pressure and temperature measurements, and it included flow screens. The total pressure (P_0) was measured at the nozzle exit with a simple impact tube. Thermocouples were used to measure the air total temperature (T_0) within the main calibrator chamber and against the endwall of the cavity (T_w).

The cavities were made by drilling holes through various thicknesses of Plexiglas. A cover plate with an epoxy mounted thermocouple was placed over one end of the cavity. The open end faced the normal impinging jet. Cavity diameters varied from 0.24 cm to 0.95 cm and lengths varied from 0.32 cm to 2.54 cm. Each cavity was located at 1.14 cm from the nozzle exit during measurements.

A series of tests were carried out for the jet total pressure (P_0) varying from 34.5 kN/m^2 to 2.1 kN/m^2. Surrounding temperatures generally remained within 0.3 °C of the jet total temperature. Initially it was discovered that certain combinations of jet total pressure beyond critical flow (79.6 kN/m^2 gauge) and cavity length produced the resonating whistle with temperature differences as high as 235 °C.

The main interest in this study is the non-resonant condition. Temperature increases in non-resonating cavities are shown in figures 2 and 3 for various D/d ratios, cavity lengths, and jet total pressures. The temperature difference ($T_w - T_0$) increased with the total pressure up to the critical pressure. At higher pressure the particular expansion cell at the cavity mouth changed with the pressure, and the pressure trend was mixed. It is seen in the figures that the temperature difference peaks between D/d ratios of 1.25 and 1.50, for all pressures, cavity lengths and cavity diameters. At higher pressures the flow generates supersonic expansion cells whose characteristics change with the pressure ratio. Thus, the distance separating the nozzle and the cavity becomes important, and the pressure trend is mixed. The most important finding is that the temperature difference peaks at $D/d = 1.25$ to 1.5 for all pressures, cavity lengths, and cavity diameters. This supports the idea that a strong vortex may be present and necessary to generate the heating effects. Although it would be expected that cavity length to diameter ratios near one would promote

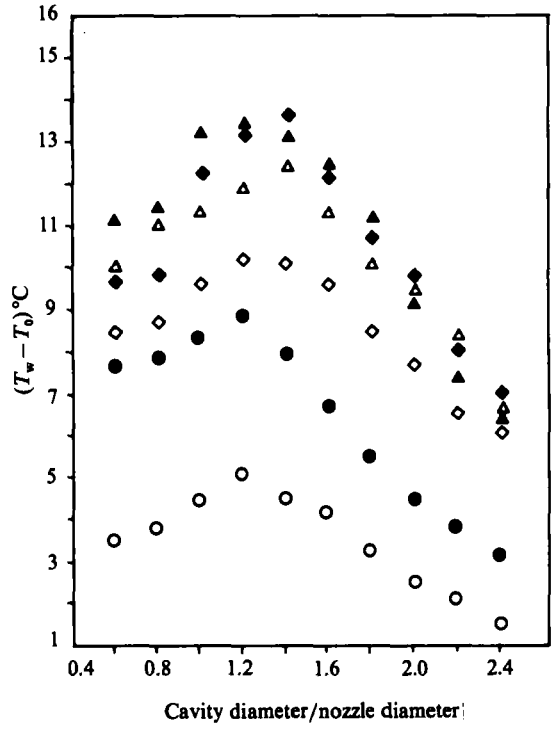

FIGURE 2. Cavity wall temperature above the jet stagnation temperature. Cavity length is 0.63 cm. P_0 (N/m² gauge): ○, 0.345×10^5; ●, 0.689×10^5; ◇, 1.034×10^5; ◆, 1.379×10^5; △, 1.724×10^5; ▲, 2.068×10^5.

stronger vortices and higher temperatures at the endwall, the data shows only minor variation with cavity length. Repeatability of the data is reflected in the consistent trend from one cavity diameter to another.

2.2. *Flow visualization*

A flow-visualization study was conducted to verify the presence of a vortex pattern in the cavities. Two cavities were made from Plexiglas tubing with D/d ratios of 3.1 and 1.5. The larger nozzle of 1.65 cm in diameter was used in the flow visualization studies. The axes of the jet and cavity were aligned with each other. Smoke was injected behind the screens in the main chamber of the calibrator leaving the nozzle smoothly at $R = 850$, the limiting Reynolds number for laminar flow. Figures 4 and 5 show the nozzle on the left and the cavity on the right. A narrow slot of high-intensity light in a darkened room illuminated the smoke.

Figure 4 shows a photograph of the flow pattern in the cavity with the D/d ratio of 3.1. Small vortices are present in the corners where the flow reverses. During the investigation using the cavity with D/d ratio of 1.5, a striking pattern occurred (figure 5). The entire central region of the cavity was dominated by a single cylindrical vortex, rotating with its axis perpendicular to the jet–cavity axis. Smoke filaments within the cavity moved quickly from the outside to the centre where the distinct rings persisted after the smoke ceased from the nozzle. The figure also shows that the vortex rotation could be clockwise or counterclockwise. The direction of

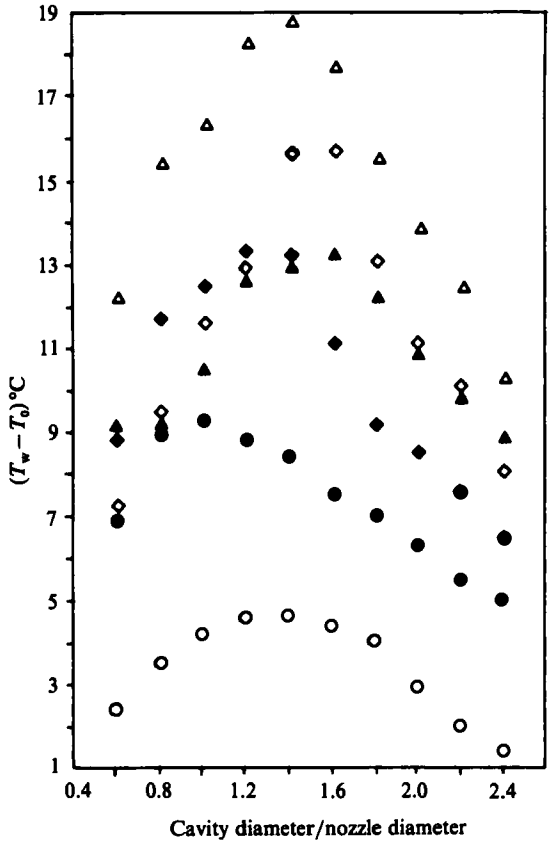

FIGURE 3. Cavity wall temperature above the jet stagnation temperature. Cavity length is 1.27 cm. See figure 2 for key.

rotation was determined by the unavoidable slight non-alignment of the jet axis and the cavity axis.

2.3. *Cavity interior measurements*

The velocities, temperatures, and pressures were measured using a Plexiglas cavity with D/d ratio of 1.5 and L/d ratio of 1.2. The cavity was placed 5.0 cm downstream from the 1.65 cm diameter jet nozzle. The probe was inserted through a parallel slot cut along the cavity length parallel to the cavity axis. The exposed portion of the slot was covered with tape. Investigations disclosed that a non-alignment up to 10% between the nozzle axis and cavity axis will not change the temperature at the end-wall of the cavity. Thus, a deliberate slight non-alignment in a preferred direction assured that the probes would be located in the plane of the vortex.

All tests were conducted with a jet nozzle velocity of 74 m/s. A TSI Model 1054-A constant temperature linearized anemometer was used for velocity measurements. A TSI Model 1260 hot-wire (0.125 cm) probe was placed perpendicular to the flow in the plane of the vortex. A copper–constantan thermocouple was used for temperature measurements. An impact tube was used for pressure measurements. The cavity was divided into a 12×12 matrix for point locations of the probes. Initial studies of realigning the jet and cavity, and reinserting the probes, suggested an

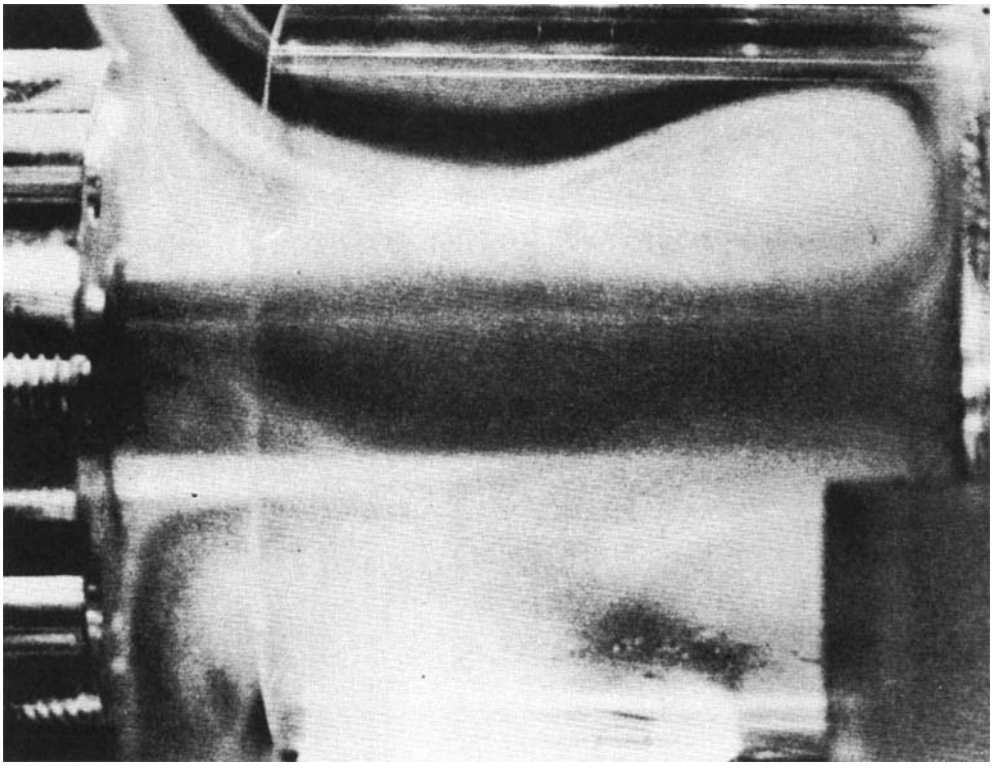

FIGURE 4. Smoke patterns in a cavity 5.1 cm in length and 5.1 cm in diameter.

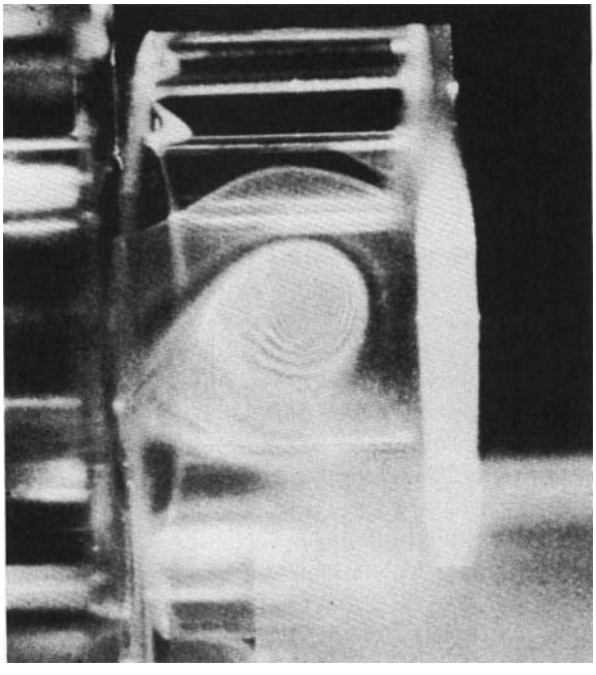

FIGURE 5. Smoke patterns in a cavity 1.65 cm in length and 2.54 cm in diameter.

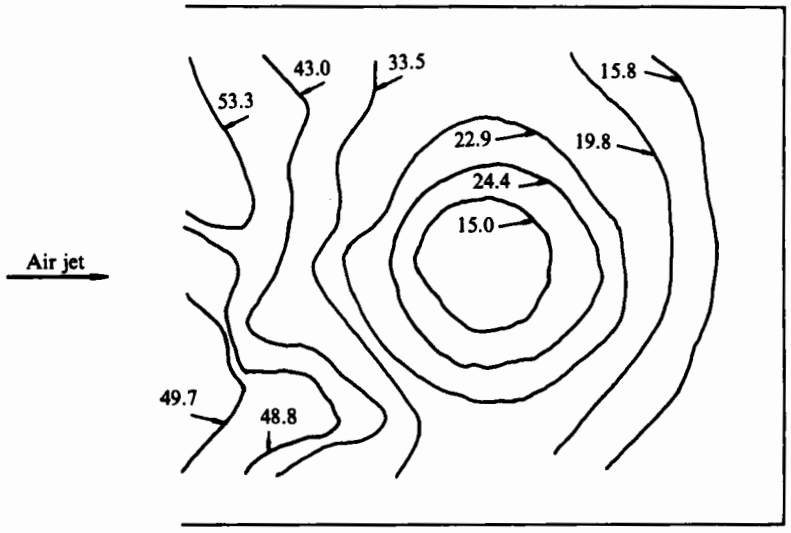

FIGURE 6. Velocity contours in a cavity 3.05 cm in length and 2.54 cm in diameter (m/s).

uncertainty in repeated measurements for velocity, pressure, and temperature of 5–10 %. Measurements at the wall were consistently repeated to within 5 %.

The results of the velocity measurements are shown in figure 6 as contour lines of constant mean velocity. Detailed turbulence measurements were not undertaken, but an exploratory study disclosed turbulence levels 10–15 % of the mean flow with the higher values near the cavity top. The vortex pattern in the cavity centre is very evident although some distortion exists near the impinging jet entrance on the left. The average velocity in the vortex increased from the centre to a maximum ($U_{\max}/U_{\text{jet}} = 0.33$) before decaying slowly. A large velocity gradient existed near the wall. Some averaging effect caused by the finite size of the wire is certainly present. Subsequent flow-visualization studies with the probe inserted in the cavity did not change the flow pattern. However, it was observed that the vortex pattern (and centre) oscillated with small amplitude as though it were buffeted by the jet.

The total temperature (T_0) in a moving air stream can be determined from the relation (Moffat 1962)

$$T_0 = T_j[1-0.5M^2(1-F)(k-1)/(1+0.5M^2(k-1))]^{-1}, \tag{2.1}$$

where T_j is the thermocouple temperature, M is the flow Mach number, F is the thermocouple recovery factor, and k is the ratio of specific heat at constant pressure (c_p) to the specific heat at constant volume (c_v).

The recovery factor was found from measurements at the nozzle exit and using the relation

$$F = 1-[(1-T_j/T_0)(P_0/P)^{(k-1)/k}][(P_0/P)^{(k-1)/k}-1]^{-1}, \tag{2.2}$$

where P_0/P is the ratio of total pressure to static pressure.

Measured recovery factors over the subsonic Mach number range were 0.86 for the probe parallel to the flow and 0.70 for the probe normal to the flow. These results were in agreement with Moffat (1962).

The static temperature was obtained from the relation

$$T = T_j[1+0.5FM^2(k-1)]^{-1}. \tag{2.3}$$

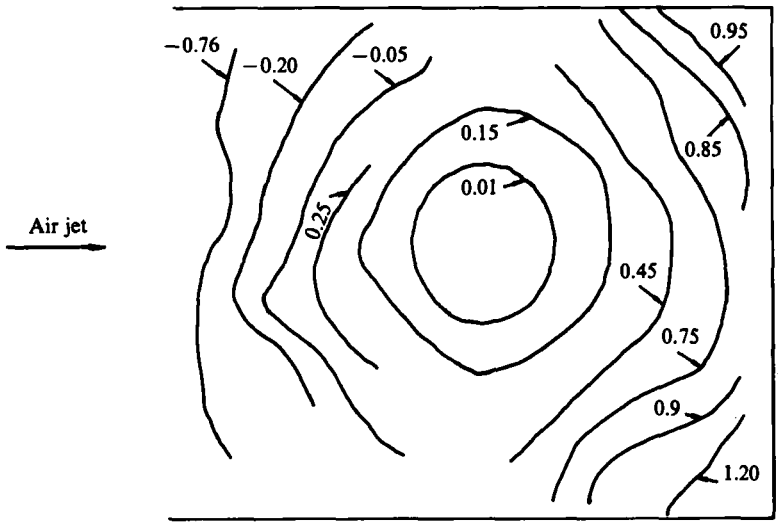

FIGURE 7. Contours of static temperature in a cavity minus stagnation temperature of the jet (°C). Cavity is 3.05 cm in length and 2.54 cm in diameter.

Figure 7 shows the static temperature contours inside the cavity, referenced to the jet total temperature, T_0. Temperatures were based upon (2.3) using the smaller recovery factor. The temperature contours have the same pattern as the velocity contours and appear more uniform. The central portion of the vortex had a constant static temperature equal to the jet total temperature. This finding is consistent with the core temperature in Ranque–Hilsch tubes when the hot-air valve is closed (Sibulkin 1962).

Finally the thermocouple temperature was recorded at the vortex centre and simultaneously at the bottom wall where the velocity is zero. The difference $(T_w - T_c)$ between the centre and the endwall is 1.08 °C. Repeated measurements over several days were within 3 %. When the core reading is corrected for the velocity using (2.3) the difference becomes 1.24 °C.

3. Vortex theory

3.1. *Ideal vortex*

In keeping with the simple vortex theory in cylindrical coordinates (r, θ, z) no property changes occur in the θ-direction or in the axial direction.

The steady state continuity equation is

$$\frac{(1/r)\partial(r\rho U_r)}{\partial r} = 0 \quad \text{(continuity)}, \tag{3.1}$$

Either $r\rho U_r$ is constant or $U_r = 0$. The latter is consistent with the concept of an ideal vortex in which no source is present at the centre. It is also consistent with the well-defined smoke cells in the flow-visualization experiments.

The momentum equations under the above assumptions reduce to

$$\frac{\rho U_\theta^2}{r} = \frac{\mathrm{d}P}{\mathrm{d}r} \quad (r\text{-momentum}), \tag{3.2}$$

which gives the pressure distribution throughout the vortex, and

$$0 = \frac{\partial \tau}{\partial r} + \frac{2\tau}{r} \quad (\theta\text{-momentum}), \tag{3.3}$$

where

$$\tau = -\rho \epsilon_{\mathrm{M}} \left(\frac{\partial U_\theta}{\partial r} - \frac{U_\theta}{r} \right),$$

and $\rho \epsilon_{\mathrm{M}}$ is the eddy viscosity, constant for vortex flow as proposed by Deissler & Perlmutter (1960).

The solution of (3.3) takes the form

$$U_\theta = \frac{C_1}{r} \quad \text{(free vortex)}, \tag{3.4}$$

$$U_\theta = C_2 r \quad \text{(forced vortex)}, \tag{3.5}$$

where C_1 and C_2 are constants, and U_θ is tangential velocity in the vortex at radius R.

This solution presents the well-known Rankine combined vortex (Duncan, Thom & Young 1975), in which the central region is a forced vortex and outer region is a free vortex. If the maximum velocity (U_{m}) is at $r = r_{\mathrm{m}}$ then

$$\left.\begin{aligned} U_\theta &= \frac{U_{\mathrm{m}} r}{r_{\mathrm{m}}} \quad (0 \leqslant r \leqslant r_{\mathrm{m}}), \\ U_\theta &= \frac{U_{\mathrm{m}} r_{\mathrm{m}}}{r} \quad (r_{\mathrm{m}} \leqslant r \leqslant r_{\mathrm{d}}). \end{aligned}\right\} \tag{3.6}$$

To explain the heating effect the authors were drawn to the Ranque–Hilsch tube and the proposed mechanism of turbulent packets subjected to thermodynamic cycling in the radial pressure gradients. Hinze (1975) has modified the energy equation to include this turbulent heating:

$$\left(\frac{1}{r}\right) \mathrm{d}\left[r \left(\frac{c_p \, \mathrm{d}T}{\mathrm{d}r} - \frac{U_\theta^2}{r} \right) \right] \Big/ \mathrm{d}r + Pr_{\mathrm{t}} \left(\frac{\mathrm{d}U_\theta}{\mathrm{d}r} - \frac{U_\theta}{r} \right)^2 = 0, \tag{3.7}$$

where the second term in the first bracket is the 'Hilsch effect', and Pr_{t} is the Prandtl number. Substituting the velocity profile from equation (3.6) and applying the following boundary conditions:

1. $T(r)$ is finite $(0 \leqslant r \leqslant r_\infty)$
2. $T(0) = T_{\mathrm{c}}$,
3. $T(r_{\mathrm{m}}^-) = T(r_{\mathrm{m}}^+)$,

the solution for the temperature distribution is

$$\left.\begin{aligned} T - T_{\mathrm{c}} &= 0.5 E_{\mathrm{m}} \left(\frac{r^2}{r_{\mathrm{m}}^2} \right) \quad (0 \leqslant r \leqslant r_{\mathrm{m}}), \\ T - T_{\mathrm{c}} &= E_{\mathrm{m}} Pr_{\mathrm{t}} \left(\frac{1 - r_{\mathrm{m}}^2}{r^2} \right) + E_{\mathrm{m}} \left(\frac{1 - r_{\mathrm{m}}^2}{2r^2} \right) \quad (r_{\mathrm{m}} \leqslant r \leqslant r_\infty), \end{aligned}\right\} \tag{3.8}$$

where

$$E_{\mathrm{m}} = \frac{U_{\mathrm{m}}^2}{c_p}.$$

At large radii from the vortex centre the temperature approaches

$$T_\infty - T_{\mathrm{c}} = E_{\mathrm{m}}(Pr_{\mathrm{t}} + 1). \tag{3.9}$$

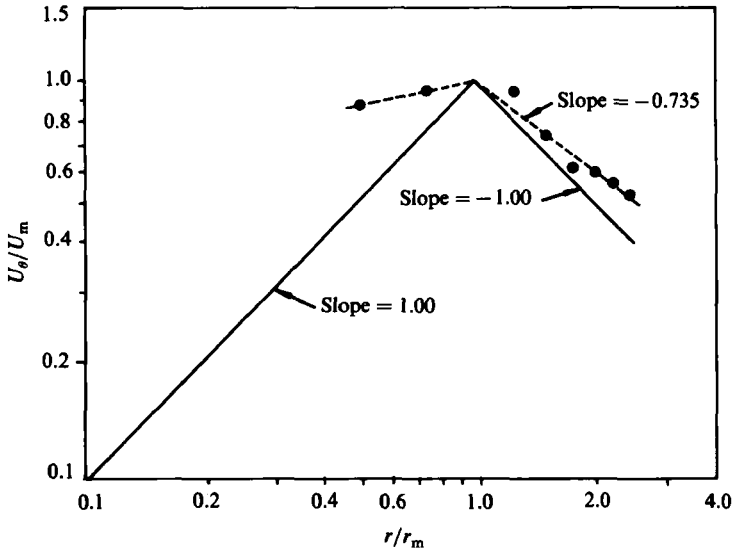

FIGURE 8. Experimental and theoretical tangential velocity in the vortex. ——, ideal vortex; – – ● – –, experiment.

It is noted that the Prandtl number, $Pr_t = 0.86$ from Kays & Crawford (1978), represents the temperature increase due to viscous heating while the unity term represents the Hilsch effect.

Substituting the velocity profile from (3.6) into (3.2) and matching the two solutions at r_m, the pressure distribution in the vortex is

$$\left.\begin{aligned} P-P_c &= \frac{\rho U_m^2 r^2}{2r_m^2} \quad (0 \leqslant r \leqslant r_m), \\ P-P_c &= \rho U_m^2\left(1-\frac{r_m^2}{2r^2}\right) \quad (r_m \leqslant r \leqslant r_\infty). \end{aligned}\right\} \tag{3.10}$$

3.2. *Actual vortex*

The actual flow is bounded by walls; therefore, the vortex velocities will not necessarily follow the ideal flow. When measuring mean velocities in hydrocyclone separators, Kelsall (1952) found that the inner forced vortex obeys (3.5) while the outer free vortex velocity decays with a slope (calculated by authors) $m = 0.75$ rather than the ideal slope $m = 1.0$. Figure 8 shows the mean velocity across the central plane of the cavity. Although the uncertainty of the core velocity measurements is evident, the free vortex velocities are in agreement with Kelsall. The more realistic velocity profile comparable to (3.6) is

$$\left.\begin{aligned} U_\theta &= \frac{U_m r}{r_m} \quad (0 \leqslant r \leqslant r_m), \\ U_\theta &= U_m\left(\frac{r_m}{r}\right)^m \quad (r_m \leqslant r \leqslant r_d), \end{aligned}\right\} \tag{3.11}$$

where r_d is equal to the cavity radius (r_w) minus the boundary-layer thickness δ.

No velocity measurements were made next to the wall where the velocity drops sharply. The effect of boundary layer δ is estimated by modelling the corner as

stagnation flow (Hiemenz flow). Fitting an exponential curve to the computational solution given in Schlichting (1979)

$$U_\theta = U_\mathrm{d}[1-\mathrm{e}^{-b(1-\gamma)}]\gamma \quad (r_\mathrm{d} \leqslant r \leqslant r_\mathrm{w}), \tag{3.12}$$

where

$$U_\mathrm{d} = U_\mathrm{m}\left[\frac{r_\mathrm{m}}{r_\mathrm{d}}\right]^{0.735},$$

$$\gamma = \frac{r}{r_\mathrm{w}},$$

$$b = 1.4\left[\frac{U_\mathrm{d} r_\mathrm{d}}{\nu}\right]^{0.5},$$

$$\delta = r_\mathrm{w} - r_\mathrm{d}.$$

Boundary conditions include:

1. $T(r)$ is finite $(0 \leqslant r \leqslant r_\mathrm{w})$,
2. $T(r_\mathrm{m}^-) = T(r_\mathrm{m}^+)$,
3. $T(r_\mathrm{d}^-) = T(r_\mathrm{d}^+)$.

Substituting the velocity profile from (3.11) and (3.12) into the energy equation (3.7) and using these boundary conditions the temperature distribution in the vortex is

$$T - T_\mathrm{c} = 0.5E_\mathrm{m}\left(\frac{r}{r_\mathrm{m}}\right)^2 \quad (0 \leqslant r \leqslant r_\mathrm{m}), \tag{3.13}$$

$$T - T_\mathrm{c} = 0.5E_\mathrm{m} + 0.25\, m^{-2}\, E_\mathrm{m}[2m + Pr_\mathrm{t}(m+1)^2]\left[1-\left(\frac{r_\mathrm{m}}{r}\right)^{2m}\right] (r_\mathrm{m} \leqslant r \leqslant r_\mathrm{d}), \tag{3.14}$$

$$T - T_\mathrm{c} = 0.5E_\mathrm{d}\gamma^2 + b^{-2}\mathrm{e}^{-b(1-\gamma)}[1.75 - 1.5b\gamma + Pr_\mathrm{t}(b\gamma - 3 + 2b^{-1}\gamma^{-1})]E_\mathrm{d} + C \quad (r_\mathrm{d} \leqslant r \leqslant r_\mathrm{w}), \tag{3.15}$$

where

$$C = 0.5E_\mathrm{m} + 0.25m^{-2}E_\mathrm{m}[2m + Pr_\mathrm{t}(m+1)^2]\left[1-\left(\frac{r_\mathrm{m}}{r_\mathrm{d}}\right)^{2m}\right] - 0.5E_\mathrm{d}\gamma_\mathrm{d}^2 - b^{-2}\mathrm{e}^{-b(1-\gamma_\mathrm{d})}[1.75 - 1.5b\gamma_\mathrm{d} + Pr_\mathrm{t}(b\gamma_\mathrm{d} - 3 + 2b^{-1}\gamma_\mathrm{d}^{-1})]E_\mathrm{d},$$

$$E_\mathrm{d} = \frac{U_\mathrm{d}^2}{c_p},$$

$$\gamma_\mathrm{d} = \frac{r_\mathrm{d}}{r_\mathrm{w}},$$

and E_m has been defined in (3.8). The term $b^{-2}\mathrm{e}^{-b(1-\gamma)}$ is negligibly small. Therefore, (3.15) simplifies to

$$T - T_\mathrm{c} \approx 0.5E_\mathrm{d}(\gamma^2 - \gamma_\mathrm{d}^2) + 0.5E_\mathrm{m} + 0.25m^{-2}E_\mathrm{m}[2m + Pr_\mathrm{t}(m+1)^2]\left[1-\left(\frac{r_\mathrm{m}}{r_\mathrm{d}}\right)^{2m}\right] \quad (r_\mathrm{d} \leqslant r \leqslant r_\mathrm{w}). \tag{3.16}$$

Evaluating (3.14) at $r = r_\mathrm{d}$ and (3.16) at $r = r_\mathrm{w}$, and using the boundary-layer thickness given by

$$\delta = 1.2r_\mathrm{d}\left(\frac{U_\mathrm{d} r_\mathrm{d}}{\nu}\right)^{-0.5},$$

the temperature rise across the boundary layer is

$$T_w - T_d = \frac{\delta E_d}{r_d},$$

and is negligible. Therefore, the temperature at the cavity wall is

$$T_w - T_c \approx 0.5E_m + 0.25m^{-2}E_m[2m + Pr_t(m+1)^2]\left[1 - \left(\frac{r_m}{r_d}\right)^{2m}\right]. \tag{3.17}$$

The pressure increase from the centre of the vortex to the wall is found by integrating equation (3.2) and is given by

$$\left.\begin{aligned} P - P_c &= (\tfrac{1}{2}\rho U_m^2)\left(\frac{r}{r_m}\right)^2 \quad (0 \leqslant r \leqslant r_m), \\ P - P_c &= (\tfrac{1}{2}\rho U_m^2)\left[1 + m^{-1} - m^{-1}\left(\frac{r_m}{r}\right)^{2m}\right] \quad (r_m \leqslant r \leqslant r_w). \end{aligned}\right\} \tag{3.18}$$

4. Comparison between theory and experiment

The theory developed in §3 is compared now to the experimental data, using the temperature and pressure at the centre as the reference. Theoretical solutions for the temperature and pressure distribution are based upon knowledge of the maximum velocity (U_m) and its location (r_m) in the modified Rankine combined vortex. There is no prior criteria available in the literature on vortex flows, including hydrocyclones, which fix these quantities. It was found from the experimental velocities that U_m was 24.4 m/s at r_m equal to 0.51 cm. The distance from the boundary layer near the wall, r_d can be taken as the cavity radius (r_w): 1.27 cm. A value of 1.006 kJ/kg °C was used for specific heat (c_p) of air.

Figure 9 shows the theoretical static temperature distribution across the cavity from the vortex centre to the cavity wall. Equations (3.13) and (3.16) are used for the development of the temperature profile of the actual vortex. Experimental temperatures are in good agreement with the theory. Although the temperature uncertainty for the interior measurememts is 0.1 °C, there is sufficient confidence in the relative wall measurements to place this uncertainty at 0.05 °C. Perhaps the largest source of error in the measurements is the apparent small oscillatory behaviour of the vortex observed with the smoke experiments. It is believed that the effect on mean velocity measurement is small since the turbulence levels, which contain the ordered information, were normal. A normalized static pressure distribution is shown in figure 10. The ordinate is the Euler's number defined as

$$Eu = (P - P_c)/\rho U_m^2.$$

Equation (3.18) is used in the development of this profile. Interior pressure measurements with the Pitot tube were taken in the plane of the vortex through the vortex centre. Thus, the flow velocity direction should be perpendicular to the probe tip. Uncertainty levels for the interior measurements are 10 % full scale and are less than 5 % for the wall measurement. There is a good agreement between the theory and experiment.

The small cavities in §1.2, which are impacted with much higher velocity jets produced higher cavity temperatures. Although the only measurements possible with these cavities were the near wall pressure and temperature, a comparison with the

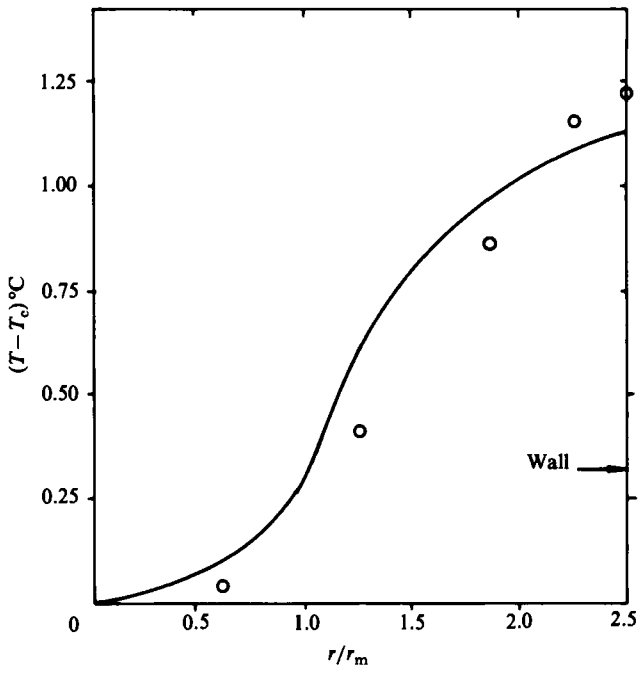

FIGURE 9. Experimental and theoretical static temperature distribution within the cavity. ——, vortex theory; ○, experiment.

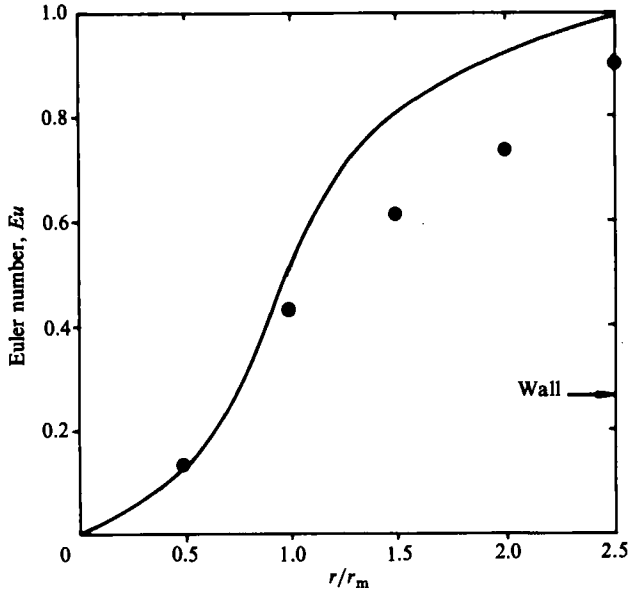

FIGURE 10. Experiment and theoretical static pressure distribution within the cavity. ——, vortex theory; ●, experiment.

large cavity results is possible by means of the Eckert number: $Ek = [E_m/T_w - T_c]$. Unlike the large cavity, the small-cavity wall pressures were found to be 90–95 % of the jet total pressure. Since the cavity pressure is the driving force on the vortex (by venting air on the weak side), the reference velocity is an adiabatic expansion of this pressure to atmosphere. All the individual Eckert numbers: (Ek) for the optimum small-cavity diameters were between 5 and 8. The Eckert number for the large cavity used for the interior measurements was 5.

5. Concluding remarks

The action of a gas jet impinging upon a cavity produces a new type of separated flow not reported previously. The complex flow within the cavity is dominated by a large central vortex described by a modified Rankine type. Similar patterns are found in Ranque–Hilsch tubes and hydrocyclones but superimposed with axial flow.

One of many mechanisms to explain the Ranque–Hilsch effect includes the adverse temperature gradient caused by turbulence within an adverse pressure gradient. The revised energy equation, which includes this mechanism, was able to predict the temperature increase from the cavity centre to the wall. The results support this explanation for Ranque–Hilsch phenomenon.

In regard to resonance tubes the oscillating movement of the shock wave at the cavity mouth causes the gas to continually charge and discharge the tube. Thus, it is probable that the transient nature of the interior flow follows a rotational path across the tube base, ideal for the Hilsch effect to be operative. Since the velocity would approach Mach one, the equivalent wall temperature using (3.17) would be 232 °C. The temperature at resonant conditions reported here as well as in other references on the Hartmann whistle agrees with this value.

REFERENCES

Broucher, E., Maresca, C. & Bournay, M. H. 1970 Fluid dynamics of resonance tubes. *J. Fluid Mech.* **43**, 389.

Brun, E. & Boucher, R. M. G. 1957 Research on the acoustic air-jet generator: a new development. *J. Acoust. Soc. Am.* **29**, 573.

Deissler, R. G. & Perlmutter, J. 1960 Analysis of the flow and energy separation in a turbulent vortex. *Intl J. Heat Mass Transfer* **1**, 173.

Duncan, W. J., Thom, A. S. & Young, A. D. 1975 *Mechanics of Fluids*, p. 24. Edward Arnold.

Hartmann, J. 1931 On the production of acoustic waves by means of an air-jet of a velocity exceeding that of sound. *Phil. Mag.* **11**, 926.

Hilsch, R. 1947 The use of the expansion of gases in a centrifugal field as cooling process. *Rev. Sci. Instrum.* **18**, 108.

Hinze, J. O. 1975 *Turbulence*, p. 477. McGraw-Hill.

Kang, S. W. 1964 Resonance tubes. PhD thesis, Renssaelaer Poly. Inst.

Kassner, R. & Knoernschild, E. 1948 Friction laws and energy transfer in circular flow. *Wright Patterson Air Force Base Tech. Rep.* no. F-TR-2198-ND.

Kays, W. M. & Crawford, M. 1978 *Convective Heat and Mass Transfer*. McGraw-Hill.

Kelsall, D. F. 1952 A study of the motion of solid particles in a hydraulic cyclone. *Trans. Inst. Chem. Eng.* **30**, 87.

Kurosaka, K. 1982 Acoustic streaming in swirling flow and the Ranque–Hilsch effect. *J. Fluid Mech.* **124**, 139.

Linderstrom-Lang, C. U. 1971 The three-dimensional distributions of tangential velocity and total temperature in vortex tubes. *J. Fluid Mech.* **45**, 161.

MOFFAT, R. J. 1962 *Temperature, Its Measurement and Control in Science and Industry*, vol. 3, part 2, p. 553.

PHILLIPS, B. R. & PAVLI, A. J. 1971 Resonance tube ignition of hydrogen–oxygen mixtures. *NASA* TN D-6354.

PRZIREMBEL, C. E. G. & FLETCHER, L. S. 1977 Aerothermodynamics of a simple resonance tube. *AIAA J.* **15**, 101.

PRZIREMBEL, C. E. G. & FLETCHER, L. S. 1978 Aerothermodynamic characteristics of a resonance tube driven by a subsonic jet. *AIAA J.* **16**, 184.

RAKOWSKY, E. L., CORRADO, A. P. & MARCHESE, V. P. 1974 Fluidic explosive initiator. *Sixth Cranfield Fluidic's Conf.* paper H4.

RANQUE, G. J. 1934 Method and apparatus for obtaining from a fluid under pressure two currents of fluids at different temperatures. *U.S. Patent*, no. 1, 952,281.

SCHLICHTING, H. 1979 *Boundary Layer Theory*, p. 95. McGraw-Hill.

SIBULKIN, M. 1962 Unsteady, viscous, circular flow, application to Ranque–Hilsch vortex tube, part 3. *J. Fluid Mech.* **14**, 269.

SIBULKIN, M. 1963 Experimental investigation of energy dissipation in a resonance tube. *Z. angew. Math. Phys.* **14**, 695.

SPRENGER, M. 1954 Ueber Thermische Effekte in Resonanzrohren. *Mitt. Inst. Aero.* **21**, 18.

STEPHAN, K., DURST, M., HUANG, F. & SEHER, D. 1983 An investigation of energy separation in a vortex tube. *Intl J. Heat Mass Transfer* **26**, 341.

THOMPSON, P. A. 1964 Jet-driven resonance tube. *AIAA J.* **2**, 1230.